The atomic structure and dynamics at the CaCO₃ vaterite–water interface: A classical molecular dynamics study

View Online   Export Citation   CrossMark

Alicia Schuitemaker, [iD] Paolo Raiteri, [iD] and Raffaella Demichelis[a] [iD]

AFFILIATIONS

Curtin Institute for Computation, The Institute for Geoscience Research (TIGeR), School of Molecular and Life Sciences, Curtin University, GPO Box U1987, 6845 Perth, Western Australia, Australia

Note: This paper is part of the JCP Special Collection in Honor of Women in Chemical Physics and Physical Chemistry.
[a]**Author to whom correspondence should be addressed:** raffaella.demichelis@curtin.edu.au

ABSTRACT

Classical molecular and lattice dynamics were applied to explore the structure and dynamics of water on different surfaces of vaterite, the least abundant calcium carbonate polymorph. Surfaces were generated starting from the three possible structural models for vaterite (monoclinic, hexagonal/trigonal, and triclinic) and pre-screened using their surface energies in an implicit solvent. Surfaces with energies lower than $0.55 \, \text{J/m}^2$ were then run in explicit water. The majority of these surfaces dissolve in less than 100 ns, highlighting the low stability of this phase in abiotic environments. Three stable surfaces were identified; they exhibited only minor structural changes when in contact with explicit water and did not show any tendency to dissolve during 1 μs molecular dynamics simulations. The computed water density profiles show that all these surfaces have two distinct hydration layers. The water residence time at the various calcium sites was computed to be within 0.7 and 20.5 ns, which suggests that specific Ca ions will be more readily available to bind with organic molecules present in solution. This analysis is a step forward in understanding the structure of this complex mineral and its role in biomineralization, as it provides a solid theoretical background to explore its surface chemistry. In particular, this study provides realistic surface models and predicts the effect of water exchange at the surface active sites on the adsorption of other molecules.

Published under license by AIP Publishing. https://doi.org/10.1063/5.0049483

I. INTRODUCTION

Vaterite is the least stable anhydrous phase of calcium carbonate (CaCO₃) at ambient pressure and temperature. Originally thought of as a rare biomineral, it has now been detected in numerous living beings. For example, vaterite is associated with the formation and repair of damaged shells (e.g., freshwater snails[1,2] and saltwater clams[3]). It is also found in freshwater pearls[4] and in the otoliths of freshwater fish.[5] Recently, vaterite has been found in common alpine plants, where it is believed to act as a light deflector.[6]

In addition to its importance in biomineralization and its potential in optical applications, vaterite has recently attracted much attention within the materials science community due to how chiral acidic amino acids can direct its growth and define its shape. In particular, L- and D-chiral acidic amino acids have been utilized to grow left- and right-handed vaterite toroids, respectively.[7] The growth of these toroids appears to be enabled by the formation of homochiral clusters of aspartic acid at the surface.[8] More broadly speaking, there are numerous experimental studies that demonstrate that organic additives can be employed to stabilize vaterite and prevent its transformation into more stable phases of CaCO₃.[9–19] Additionally, different concentrations of specific organic molecules can be used to tune the structural features (e.g., size, shape, texture, and porosity) of vaterite.[9,11,13,18,19] For example, it has been suggested that the complexation of calcium ions by glycine/glycinate in the growth solution is responsible for the formation of spherical vaterite particles, with the carbonate ions and glycine competing for the calcium ions.[14,17]

While a certain level of knowledge exists about vaterite, its growth, and its interaction with biomolecules, its surface chemistry is totally unexplored. This is due to the complexity of its structure,

TABLE I. Summary of the multiple structures of vaterite.

Hexagonal/trigonal	Monoclinic	Triclinic
$P6_522 \mid P6_122$	$C2/c$	$C-1$
$P6_5 \mid P6_1$	Cc	$C1(1)$
$P112_1$	$C2$	$C1(2)$
$P3_221 \mid P3_121$		

TABLE II. Summary of energetic data for different vaterite polytypes relative to the hexagonal/trigonal structure [ΔU(h)] and to calcite [ΔU(calcite)]. All the energies are internal energies and are reported in kJ/mol per formula unit. For the force field (FF), all the structures in one basin averaged out to the same energy and structure, while the quantum mechanical data (QM) obtained with the PBEsol functional are included for the most stable structure in the basin [i.e., C1 (t), C2 (m), and $P3_221$ (h)].

Polytype	ΔU (h)		ΔU (calcite)	
	FF	QM	FF	QM
Triclinic (t)	−0.2	+0.4	+7.2	+3.5
Monoclinic (m)	−0.1	+0.1	+7.3	+3.2
Hexagonal (h)	0.0	0.0	+7.4	+3.1

summarized in Table I and characterized by polytypism, free rotation of carbonates, and chirality.[20] In particular, vaterite exhibits multiple structures, which can be divided into two main models, namely, the monoclinic model (m) and the hexagonal/trigonal model (h). These models, which are both compatible with XRD, Raman spectroscopy, and ^{43}Ca nuclear magnetic resonance (NMR) experiments,[21–23] differ in the sequence of carbonate layers, and they both include a pool of sub-structures that can interconvert through minor rotations of carbonate anions. Some of these sub-structures are chiral. A third hypothetical polytype (triclinic, t) found through density functional theory (DFT) but not fully compatible with the experimental evidence is also reported in Table I and will be used as an additional reference structure in this paper.

To date, an unequivocal definition of what are the stable surfaces of vaterite and how they interact with water is still missing. Computer simulations have mostly been applied to gain insight into the bulk structure of vaterite.[20,21,24,25] Only a very small number of computational investigations have considered vaterite surface stabilities, all based on structural models that do not correspond to the most likely structures of vaterite, and none have considered their stability in bulk water.[26]

In order to be able to investigate the atomic details of the effect of biomolecules in directing the formation of vaterite and in shaping its appearance, a systematic study of its surface properties and of its interaction with explicit water (i.e., the reaction medium) is required. This work aims to provide this foundation. A set of stable surfaces will be provided for vaterite, within the constraints of the most recently defined structural models.[20,21,27] A quantitative analysis of the structure and dynamics of water at these surfaces will also be presented to determine to what extent the dehydration of the surface will present a major barrier for the attachment of other molecules, as in the case of calcite steps.[28]

II. COMPUTATIONAL METHODS

A. Force field parameterization and transferability

The latest force field for calcium carbonates developed by Raiteri et al.[29] was used, in combination with the SPC/Fw water model by Wu et al.[30] This force field was parameterized against experimental data for structural and thermodynamic properties of both the constituent ions in solution and in the solid phases.

Table II summarizes the transferability of this force field to vaterite, as the latter was not part of the systems used in the fitting procedure. The relative differences between the three polytype pools are on the order of 0.1–0.4 kJ mol^{-1} f.u.$^{-1}$, with both the force field and DFT. The agreement is excellent, and the differences are

largely within the error of the method. As described in the introduction and summarized in Table I, vaterite has multiple structures that can be divided into three main basins. The force field does not discriminate between vaterite models belonging to the same polytype pool, meaning that it does not identify the transition states identified through DFT.[20] Specifically, this means that $P6_522$ is a stable structure and has the same energy and structure as $P3_221$, $P112_1$, and $P6_5$. Similarly, $C2/c$ is indistinguishable in structure and energy from Cc and $C2$. The test performed on the triclinic hypothetical polytype (t) shows that $C-1$ is again identical in energy and structure to the two $C1$ structures. We also note that the force field slightly overestimates the energy difference between vaterite and calcite with respect to both the experiment (3.2 kJ mol^{-1} f.u.$^{-1}$[31]) and DFT (3.1–4.7 kJ mol^{-1} f.u.$^{-1}$ depending on the functional).

It is important to highlight that these limitations do not affect the simulations conducted in this work, as neither the bulk properties of vaterite nor its properties relative to calcite are being considered. Additionally, the rotation of the carbonate anions, which leads to structural interconversions, can be accessed at room temperature. This means that regardless of the force field ability to discriminate between the various structures within the same crystal system, molecular dynamics simulations can easily explore all states within a polytype pool.

B. Surface structure and stability

The GDIS[32] package was used to search and generate different nonpolar surface cuts from three different vaterite structures: the monoclinic structure, the trigonal structure, and the triclinic structure. The search for surfaces was conducted using all models reported in Table I. GDIS creates different crystal planes for vaterite by cleaving the structure at different points along the main crystallographic axes, i.e., creating planes with different Miller indices (hkl), which are the inverse of the intercept with the lattice vectors. As expected from the similarity of the structures within the same crystal system, their surfaces are the same. For this reason, in the text, we will use m, h, and t to indicate whether a surface belongs to a monoclinic, a hexagonal/trigonal, or a triclinic model, respectively. The initial focus was on determining all surfaces with a spacing of the molecular planes, d_{hkl}, close to the experimentally determined value of 3.6 Å.[7] The search was then expanded to any d_{hkl} values found by GDIS within the limit of the first 50 nonpolar surfaces, starting

from the largest d_{hkl} value. In addition, surfaces reported in the previous literature[12,26,33] were also considered if these were nonpolar. Within the same (hkl) family, all the possible shifts were tested. The geometry of these various cuts was optimized at constant volume using GULP,[34] in vacuum and in an implicit solvent (using the COSMIC method[35,36]), to determine the surface energies as preliminary estimates of the surface stability.

The surfaces with the lowest surface energies predicted by the COSMIC model ($\gamma_{s,a}$ < 0.55 J/m^2) were then exposed to explicit water by running unbiased molecular dynamics (MD) with the LAMMPS[37] package. A time step of 1 fs was used, and the atomic trajectories were written every 1 ps. The temperature and pressure were maintained using a chain of five Nosé–Hoover thermostats and barostats each with relaxation times of 0.1 and 1 ps, respectively.

Supercells of ~50 × 50 × 50 Å^3 were generated for the various surface models. The vaterite–water interfaces were obtained by combining the aforementioned supercells and an equilibrated box of water of the same size. This system was then equilibrated for 2 ns at ambient conditions (NPT ensemble, 300 K, and 1 bar), where the box was allowed to relax independently in all directions. Production runs were preformed within an NVT ensemble at 300 K and run for up to 1 μs, unless surface dissolution occurred first.

C. Structure and dynamics of water at the interface

The MD trajectories for the stable vaterite surfaces were used to analyze the water density maps (1D and 3D), the pair distribution functions (PDFs), and the residence times of water above the calcium ions on the surface using the GPTA.[38]

Pair distribution functions for different calcium sites provide important information about the solvation structure of the ions. The main feature of interest is the first peak, which can be used to estimate the average number of water molecules coordinated with a given site in the first solvation shell. This is achieved using the following equation:

$$n(r) = \int \rho g(r) dV = \int 4\pi r^2 \rho g(r) dr. \tag{1}$$

The first minimum also provides the cutoff point for the first solvation shell. This is required for the determination of the average water residence times.

The average residence time of water molecules on different calcium sites was determined using a survival function $P(t)$. $P(t)$ is an integral of the distribution function $[E(t)]$ as seen in the following equation:[39]

$$P(t) = \int_t^\infty E(t') dt'. \tag{2}$$

$E(t)dt$ represents the likelihood that a water molecule is coordinated with a given calcium ion for a certain timespan between t and $t + dt$. The probability that a water molecule will remain coordinated for at least within t and $t + dt$ is equivalent to $1/\tau \, P(t)dt$, where τ is the average residence time.

Analogous to a previous work on calcite,[28] the average water residence time at the calcium site was determined by fitting the survival function against a sum of decaying exponential functions as

shown in the following equation:[40]

$$P(t) = \sum_{i=1}^m a_i e^{-t/\tau_i}, \tag{3}$$

where m is the number of water molecules present in the calcium's first hydration shell, which was determined by integrating the first peak of the PDFs. As the minimum in the PDFs between the first and second peaks does not always reach zero, in some cases, an additional exponential function was added to improve the fitting. This extra function accounts for the fact that some water molecules in the second solvation shell can be included in the calculation of the survival function due to thermal vibrations, which bring them inside the cutoff radius used to determine whether the molecule is coordinated with the Ca site or not (≈3.7 Å). However, because those molecules are not part of the first coordination shell of Ca, their residence time is very short (few tens of ps), and the inclusion of this extra function does not affect the fitting of the survival function at the longer time scales.

III. RESULTS AND DISCUSSION

A. Stability of different vaterite surfaces

The surface energies of the first 50 nonpolar surfaces starting from the highest d_{hkl} value for each of the structures were calculated in vacuum ($\gamma_{s,g}$) and in an implicit solvent ($\gamma_{s,a}$). The results are reported in Tables S1–S6 in the supplementary material. Then, the stability of all the surfaces with $\gamma_{s,a}$ < 0.55 J/m^2 was further tested by performing extensive molecular dynamics simulations in an explicit solvent using LAMMPS.

For d_{hkl} depths close to the experimental value of 3.6 Å,[7] four nonpolar surfaces were found with the chosen surface energy cutoff; three belonged to the monoclinic basin [(−311), (01−2), and (020)] and the remaining one to the hexagonal basin [(110)]. All these surfaces are microfaceted and rough. Only the (020)m surface remained stable after being exposed to explicit water for an extended time period (>100 ns), while the others readily dissolved. For these unstable surfaces, we observed water molecules percolating into the surfaces within a few tens of ns and several surface ions detaching. The monoclinic (020) surface remained stable throughout a >1 μs MD simulation. However, after about 650 ns of MD, one water molecule penetrated into the surface, which led to distortion of the carbonate ions near the adsorption site. A second independent simulation was set up for this surface, and a similar event was observed at a different site after 690 ns. Although in both cases the surface remained overall stable for the remainder of the simulation, these observations suggest that the water incorporation in (020)m is a possible, albeit rare, event, and if enough water molecules enter the surface, it could lead to a reorganization or the dissolution of the surface itself. A complete characterization of this phenomenon is, however, beyond what can be achieved by unbiased MD simulations, and for the purpose of this work, the (020)m surface will be considered stable, and all the analysis will be performed by ignoring the sites close to the incorporated water molecule.

After exploring the stability of the surfaces close to the experimental d_{hkl} value, the search was extended to other d_{hkl} depths. This resulted in the testing of further 33, 12, and 14 cuts from the monoclinic, trigonal/hexagonal, and triclinic models, respectively. Most

of these surfaces also had a rough topology, which allowed water molecules to enter the surface and ultimately dissolve it before reaching 100 ns of MD. The surface energies computed for the surfaces that did not dissolve within the first 100 ns of MD simulation are summarized in Table III. Only one of these four surfaces was from the trigonal/hexagonal basin [(200)], while the others were from the monoclinic basin [(31−3), (022), and (111)]. Upon extending the simulations beyond 100 ns, only (31−3)m remained stable for the full μs of MD, whereas (111)m and (022)m started to dissolve after ~120 and 240 ns, respectively. These two monoclinic surfaces were not considered further in this work. (200)h also did not dissolve before 1 μs, but water molecules were able to occasionally penetrate the surface, which distorted carbonate ions and in one case led to the temporary detachment of a calcium ion. Therefore, from this work, it appears that (31−3)m is the most stable surface, as it neither dissolves nor incorporates water at any point in 1 μs simulations. This could indicate that it may be the most likely surface to be observed experimentally, if vaterite is produced in the absence of additives. Although far from a perfect and stable surface model, all these surfaces could be used in future work to explore the binding strength and stabilizing effect of biomolecules on vaterite.

B. Water structure and dynamics on stable surfaces

The water structure of the three vaterite surfaces that remained structurally stable for at least 1 μs, (31−3)m, (020)m, and (200)h, was analyzed by computing the 1D and 3D atomic number density profiles (Fig. 1). Due to the rugged nature of the vaterite surface, there are no well separated peaks in the 1D density profiles, as it has been extensively reported for calcite.[41,42] Moreover, it can be seen that the water density profiles partially overlap with the peaks corresponding to the surface Ca ions. However, this is not an indication of any dissolution events, but it is simply due to the microfaceted nature of the vaterite surfaces, which is followed by the hydration layers. In fact, the 3D density maps clearly show regions of high probability density for the water oxygen atoms that are in the first solvation shell of

TABLE III. Summary of data obtained using GULP for the most stable surfaces of vaterite in an aqueous environment. Included are the name of the plane, its depth (D_{hkl}) and shift, and its surface energy in vacuum ($\gamma_{s,g}$) and in an implicit solvent ($\gamma_{s,a}$). Furthermore, the decrease in surface energy due to the presence of the implicit solvent ($\Delta\gamma_{s,g\rightarrow a}$) was also determined. D_{hkl} and the energies are given in Å and J/m^2, respectively.

Surface	D_{hkl}	$\gamma_{s,g}$	$\gamma_{s,a}$	$\Delta\gamma_{s,g\rightarrow a}$
(31−3)m[a]	2.6934	1.077	0.491	0.586
(022)m[b]	2.7225	1.093	0.504	0.589
(020)m[a]	3.6063	1.053	0.405	0.648
(111)m[c]	4.4282	1.084	0.484	0.599
(200)h[d]	3.1139	0.725	0.358	0.367
Expt.[e]	3.6			

[a]Did not dissolve.
[b]Dissolved after 240 ns.
[c]Dissolved after 120 ns; water percolated into the surface at 65 ns.
[d]Did not dissolve; water molecules moved in and out of the surface.
[e]Reference 7.

the Ca ions or hydrogen bonded to the surface carbonate ions, in a similar fashion to what was observed for calcite.[43]

After having examined the water structure above the whole surface, the next step was to explore the hydration at the calcium ions on the surface. Similar to the water structure, this was varied across the different surfaces in terms of both the number of unique calcium sites and variation of the residence times of water molecules at these sites. The data for all three surfaces are summarized in Fig. 2 and Table IV.

As seen in Fig. 2, the monoclinic surface with the experimental d-spacing, (020)m, has six calcium ions in the unit cell, which are directly exposed to water. These six calcium sites can be subdivided into three pairs of identical sites. Site 1 ions have on average two water molecules in the first hydration shell, one of which can be shared between the two neighboring site 1 calcium ions (see Fig. 3). On the other hand, site 2 and 3 calcium ions are only associated with one water molecule on average, which is not shared as shown via trajectory snapshots in the supplementary material. The water residency time for one of the water molecules at site 1 is very fast and comparable with that of a calcium ion in solution, in other words around 200 ps.[28] The second water molecule has a longer residency time of ~1.8 ns, which is comparable to that on the basal plane of calcite (2 ± 0.2 ns[28]). The other two calcium ion sites on the surface also have a relatively low residence time of around 2.6 ns. The survival functions for this surface and the two other stable surfaces are included in the supplementary material.

The other stable surface from the monoclinic basin, (31−3)m, has 12 calcium ions in the unit cell, which are exposed to water at the interface. The peak heights of the radial distribution functions (Ca-O$_w$) are much more varied than for the other two surfaces (Fig. 2) and indicate that there are six pairs of calcium ions with the same hydration structure. The calcium ions in this surface can have as little as one and as many as five water molecules in the first solvation shell at a given point as seen from trajectory snapshots included in the supplementary material. On average, the site 1 calcium ions have 1.25 water molecules in the first hydration shell. This means that for 75% of the time, only one water molecule is coordinated with these Ca^{2+} ions, but for the remaining 25% of the time, two water molecules will be surrounding these sites. This is demonstrated by the trajectory snapshot shown in Fig. 3, where 12 and 4 of the sixteen site 1 calcium ions have one and two water molecules in the first solvation shell, respectively. Sites 2 and 3 have average water coordination numbers of very close to 1.0, i.e., for the well over 90% of time, only one water is coordinated with these sites. This can be seen from further images in the supplementary material taken from the MD trajectories. Sites 4–6 can have between three and five water molecules surrounding an individual ion at a time, as seen in the supplementary material. Sites 1–3 have no shared water molecules, but the site 4 and 5 ions can share between one and two water molecules. The water residency times for sites 1–3 are comparable to that for (020)m, ranging from 2.2 to 3.3 ns, whereas the remaining sites have much larger residence times. Sites 4 and 5 have water residence times of up to 7.2 and 9.0 ns. Site 6 has by far the slowest water exchange in this study, and the residency time for these ions is up to 20.5 ns. This is comparable with the longest water residence time determined for the acute step of calcite.[28] Such a long residency time for this site means that an adsorbing species (e.g., biomolecules or constituent ions of vaterite) would most likely have
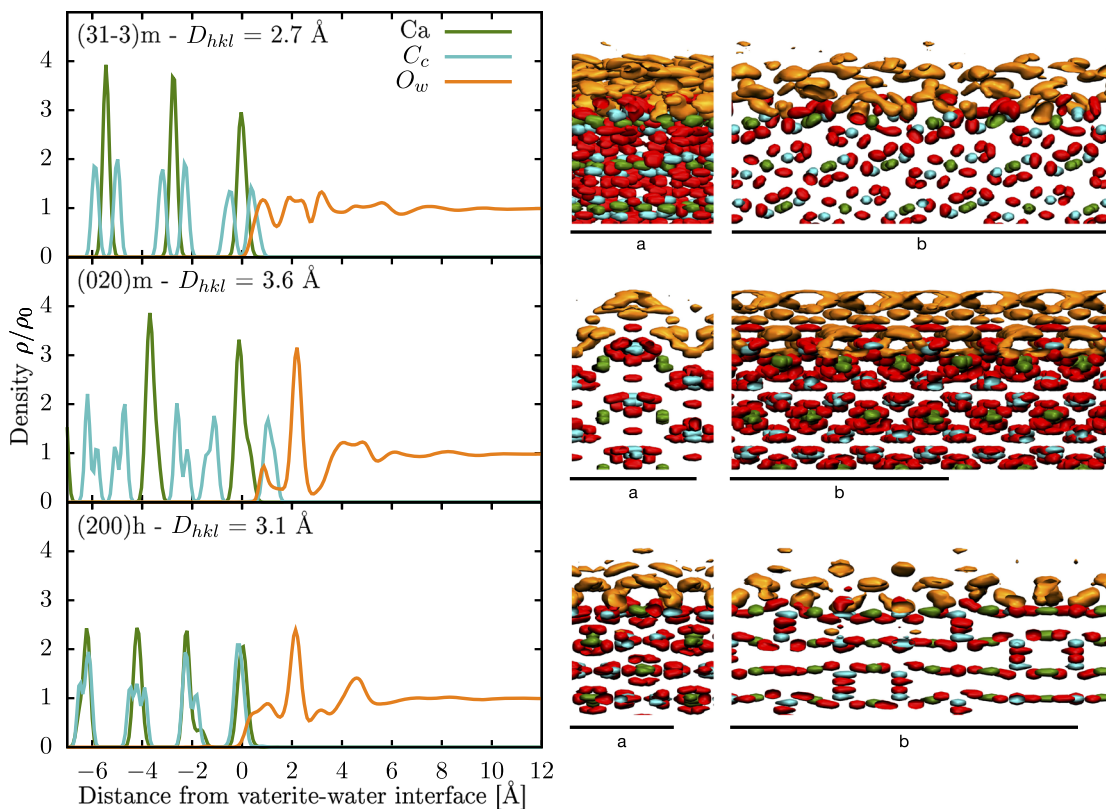
FIG. 1. 1D and 3D atomic number densities relative to the density of bulk water ρ_0 along the perpendicular of the surfaces for different vaterite–water interfaces. Calcium, carbon, and oxygen of the surface are in green, cyan, and red, respectively. The oxygen atoms of the water molecules in the ordered hydration layers are in orange. The hydrogen atoms of water are excluded for clarity on the atomic density iso-surfaces. The iso-surface values are $10\rho_0$ for the atoms of vaterite and $4\rho_0$ for the atoms of the water. The black bars on the 3D maps indicate the size of the unit cell.
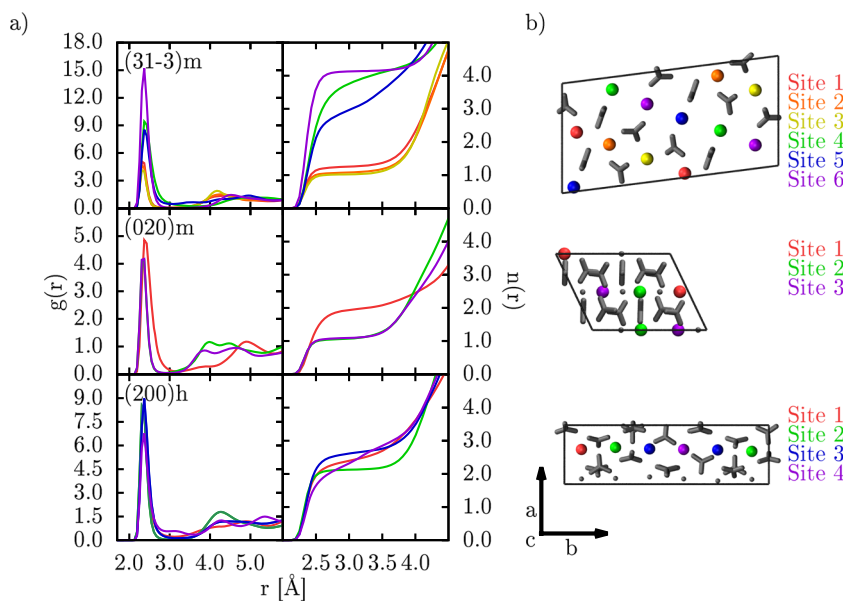

FIG. 2. (a) Water structure data for the three stable vaterite surfaces including the radial distribution functions of calcium ions with the oxygen atoms of water and the coordination number [$n(r) = \int 4\pi r^2 \rho g(r) dr$] and (b) an image of the corresponding unit cells. The data from top to bottom are for the $(31-3)$m, (020)m, and (200)h surfaces in order. The calcium ions in the unit cell images are colored based on their site number.
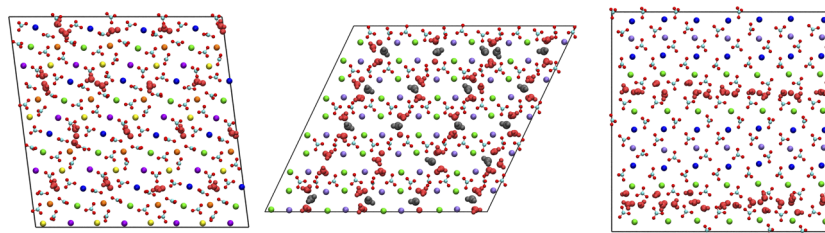
FIG. 3. Trajectory snapshots showing the water molecules coordinated with site 1 for (31−3)m, (020)m, and (200)h from left to right, respectively. For clarity, only the top layer of the vaterite surface is shown. The calcium ions are colored according to their site number, whereas carbon and oxygen are depicted in cyan and red, respectively. The red water molecules are coordinated with site 1, only one calcium ion, whereas those in gray are shared between neighboring sites.

to overcome large barriers to associate with these particular surface sites, as removal of the binding water molecule and the dehydration of this site would be associated with a high energy cost.

The last surface for which the interfacial water dynamics were explored is (200)h. This surface has a rectangular unit cell with six calcium ions exposed to water molecules at the interface as seen in Fig. 2. Unlike for the other surfaces, not all calcium ions can be paired up as seen from the pair distribution functions and the residence times obtained using the survival functions reported in the supplementary material. As can be seen in Table IV, the average water coordination number in the first hydration shell for all the surface sites is between 2 and 3 water molecules. For example, as seen in Fig. 3, site 1 calcium ions are surrounded by two and three water molecules for ~57% and 43% of the time, respectively. In this particular snapshot, 8 of the 14 site 1 ions are coordinated with two water molecules, while the remaining four have the water molecules in the first solvation shell. These are the calcium ions with the shortest residency time of about 700 ps. From sites 2–4, the average number of water molecules coordinated with the calcium ions in their first solvation shell increases, i.e., sites 3 and 4 are associated with three water molecules at the same time more frequently. The residence time also increases from 1.4 ns for site 2 to 4.3 ns for site 4. As for the other surface, some of the calcium ions have shared water molecules. Specifically, as seen in the snapshot in the

supplementary material, sites 1 and 2, as well as sites 3 and 4, have the same water molecules in their first hydration shell. Sites 2 and 3 do not appear to have water molecules in common. What makes this surface interesting and unique compared to the two other surfaces is not only that it derives from the trigonal/hexagonal basin but also that on several occasions during the simulation, water molecules would enter the surface and associate with the calcium ions in the second layer for a few nanoseconds before returning to bulk water. This leads to a distortion of some of the carbonate ions, with the maximum distortion from the average carbon position up to 2.9 Å in one case. Although usually this distortion is closer to 1.6 Å from the average position, one calcium ion is temporarily pushed out of the surface by one water molecule but returns to the surface, and the further point from the average calcium position is 6.8 Å. Unlike with the majority of the surfaces, however, this does not result in the dissolution of the surface. Future work is required to determine if this is an actual feature or an artifact of the force field by using higher level computational methods (e.g., *ab initio* MD or polarizable AMEBA force field for $CaCO_3$[44]).

IV. CONCLUSIONS

A small set of vaterite surfaces—(020)m, (31−3)m, and (200)h—that are stable in water has been identified and characterized. These surface models are compatible with the available experimental data and theoretical structural models for bulk vaterite and can be used to investigate interface processes. The high instability exhibited by the majority of the surfaces considered in this study in pure water (>50) is compatible with the fact that vaterite is predominantly found in biological environments. The dynamics at the vaterite–water interface has been explored, providing a detailed analysis of the symmetrically independent calcium sites, including the residence time of water molecules on these sites.

Overall, the three surfaces have very varied water structures and therefore dynamics. The various residence times for each of the surfaces are summarized in Table IV. This illustrates that although the water dynamics at (020)m is most likely a limited hindrance for other molecules attaching to this vaterite surface, the same molecules might face substantial barriers attempting to associate with (31−3)m and (200)h at certain calcium sites. Therefore, any computational studies aiming to access the adsorption energies of other molecular species need to take the slow water exchange into account.

This study also shows the importance of working with explicit water when examining the stability of mineral surfaces. Without using water explicitly, it would not be possible to observe water

TABLE IV. Summary of the water properties above the stable surfaces of vaterite.

	Site	No. of H_2O	Cutoff (Å)	τ_{max} (ns)
(31−3)m	1	1.25	2.97	~2.15
	2	1.07	2.91	~2.59
	3	1.02	2.97	~3.29
	4	4.19	3.69	~7.17
	5	3.01	3.03	~8.98
	6	4.15	3.21	~20.46
(020)m	1	1.98	3.21	~1.77
	2	1.08	2.85	~2.49
	3	1.03	2.97	~2.59
(200)h	1	2.43	3.09	~0.70
	2	2.13	3.09	~1.38
	3	2.66	3.21	~3.49
	4	2.91	3.57	~4.34

molecules penetrating the surfaces and pushing the surface ions out. In adddition, it highlights that working with flexible models is key to avoiding incorrect conclusions from rigid body calculations, as the equilibria at the surface are highly dynamics and complex, especially for rough surfaces. For example, (03−2)h has the lowest surface energy in the implicit solvent (0.243 J/m^2), but it dissolves very quickly when exposed to the explicit solvent. On the other hand, the surfaces that survive in explicit water have varied and higher surface energies in the implicit solvent, ranging between 0.358 and 0.491 J/m^2.

SUPPLEMENTARY MATERIAL

See the supplementary material for all surface energy data computed with GULP, images of the three stable surfaces showing their structures and water coordination, and the survival functions used to estimate the average residence time.

DEDICATION

This work is dedicated to Associate Professor Carla Roetti, a pioneer in *ab initio* simulation of solids, who tirelessly reminded to everyone working in and visiting her group what team work is, who did not miss a chance to inspire people—in her own very peculiar way—to aim at the best, in life, in our society, in coding practices, and in research ethics.

ACKNOWLEDGMENTS

DATA AVAILABILITY

The data that support the findings of this study are available within the article and its supplementary material.

REFERENCES

[1] K. M. Wilbur and N. Watabe, "Experimental studies on calcification in molluscs and the alga *Coccolithus huxleyi*," Ann. N. Y. Acad. Sci. **109**, 82–112 (1963).

[2] B. Hasse, H. Ehrenberg, J. C. Marxen, W. Becker, and M. Epple, "Calcium carbonate modifications in the mineralized shell of the freshwater snail *Biomphalaria glabrata*," Chem. - Eur. J. **6**, 3679–3685 (2000).

[3] G. Nehrke, H. Poigner, D. Wilhelms-Dick, T. Brey, and D. Abele, "Coexistence of three calcium carbonate polymorphs in the shell of the Antarctic clam *Laternula elliptica*," Geochem., Geophys., Geosyst. **13**, Q05014, https://doi.org/10.1029/2011gc003996 (2012).

[4] L. Qiao, Q.-L. Feng, and Z. Li, "Special vaterite found in freshwater lackluster pearls," Cryst. Growth Des. **7**, 275–279 (2007).

[5] D. Lenaz, M. Miletic, E. Pizzul, S. Vanzo, and G. Adami, "Mineralogy and geochemistry of otoliths in freshwater fish from Northern Italy," Eur. J. Mineral. **18**, 143–148 (2006).

[6] R. Wightman, S. Wallis, and P. Aston, "Leaf margin organisation and the existence of vaterite-producing hydathodes in the alpine plant *Saxifraga scardica*," Flora **241**, 27–34 (2018).

[7] W. Jiang, M. S. Pacella, D. Athanasiadou, V. Nelea, H. Vali, R. M. Hazen, J. J. Gray, and M. D. McKee, "Chiral acidic amino acids induce chiral hierarchical structure in calcium carbonate," Nat. Commun. **8**, 15066 (2017).

[8] W. Jiang, D. Athanasiadou, S. Zhang, R. Demichelis, K. B. Koziara, P. Raiteri, V. Nelea, W. Mi, J.-A. Ma, J. D. Gale, and M. D. McKee, "Homochirality in biomineral suprastructures induced by assembly of single-enantiomer amino acids from a nonracemic mixture," Nat. Commun. **10**, 2318 (2019).

[9] S. D. Sims, J. M. Didymus, and S. Mann, "Habit modification in synthetic crystals of aragonite and vaterite," J. Chem. Soc., Chem. Commun. **1995**, 1031–1032.

[10] H. Wei, Q. Shen, Y. Zhao, Y. Zhou, D. Wang, and D. Xu, "On the crystallization of calcium carbonate modulated by anionic surfactants," J. Cryst. Growth **279**, 439–446 (2005).

[11] Q. Shen, L. Wang, Y. Huang, J. Sun, H. Wang, Y. Zhou, and D. Wang, "Oriented aggregation and novel phase transformation of vaterite controlled by the synergistic effect of calcium dodecyl sulfate and *n*-pentanol," J. Phys. Chem. B **110**, 23148–23153 (2006).

[12] W. Hou and Q. Feng, "Morphology and formation mechanism of vaterite particles grown in glycine-containing aqueous solutions," Mater. Sci. Eng., C **26**, 644–647 (2006).

[13] A.-W. Xu, M. Antonietti, H. Cölfen, and Y.-P. Fang, "Uniform hexagonal plates of vaterite $CaCO_3$ mesocrystals formed by biomimetic mineralization," Adv. Funct. Mater. **16**, 903–908 (2006).

[14] C. Shivkumara, P. Singh, A. Gupta, and M. S. Hegde, "Synthesis of vaterite $CaCO_3$ by direct precipitation using glycine and L-alanine as directing agents," Mater. Res. Bull. **41**, 1455–1460 (2006).

[15] D. Gebauer, H. Cölfen, A. Verch, and M. Antonietti, "The multiple roles of additives in $CaCO_3$ crystallization: A quantitative case study," Adv. Mater. **21**, 435–439 (2009).

[16] Y. Su, H. Yang, W. Shi, H. Guo, Y. Zhao, and D. Wang, "Crystallization and morphological control of calcium carbonate by functionalized triblock copolymers," Colloids Surf., A **355**, 158–162 (2010).

[17] Y. Lai, L. Chen, W. Bao, Y. Ren, Y. Gao, Y. Yin, and Y. Zhao, "Glycine-mediated, selective preparation of monodisperse spherical vaterite calcium carbonate in various reaction systems," Cryst. Growth Des. **15**, 1194–1200 (2015).

[18] Y. I. Svenskaya, H. Fattah, O. A. Inozemtseva, A. G. Ivanova, S. N. Shtykov, D. A. Gorin, and B. V. Parakhonskiy, "Key parameters for size-and shape-controlled synthesis of vaterite particles," Cryst. Growth Des. **18**, 331–337 (2018).

[19] R. Sun, T. Willhammar, E. Svensson Grape, M. Strømme, and O. Cheung, "Mesoscale transformation of amorphous calcium carbonate to porous vaterite microparticles with morphology control," Cryst. Growth Des. **19**, 5075–5087 (2019).

[20] R. Demichelis, P. Raiteri, J. D. Gale, and R. Dovesi, "The multiple structures of vaterite," Cryst. Growth Des. **13**, 2247–2251 (2013).

[21] M. De La Pierre, R. Demichelis, U. Wehrmeister, D. E. Jacob, P. Raiteri, J. D. Gale, and R. Orlando, "Probing the multiple structures of vaterite through combined computational and experimental Raman spectroscopy," J. Phys. Chem. C **118**, 27493–27501 (2014).

[22] D. L. Bryce, E. B. Bultz, and D. Aebi, "Calcium-43 chemical shift tensors as probes of calcium binding environments. Insight into the structure of the vaterite $CaCO_3$ polymorph by ^{43}Ca solid-state NMR spectroscopy," J. Am. Chem. Soc. **130**, 9282–9292 (2008).

[23] K. M. N. Burgess and D. L. Bryce, "On the crystal structure of the vaterite polymorph of $CaCO_3$: A calcium-43 solid-state NMR and computational assessment," Solid State Nucl. Magn. Reson. **65**, 75–83 (2015).

[24] J. Wang and U. Becker, "Structure and carbonate orientation of vaterite ($CaCO_3$)," Am. Mineral. **94**, 380–386 (2009).

[25] R. Demichelis, P. Raiteri, J. D. Gale, and R. Dovesi, "A new structural model for disorder in vaterite from first-principles calculations," CrystEngComm **14**, 44–47 (2012).

[26] N. H. de Leeuw and S. C. Parker, "Surface structure and morphology of calcium carbonate polymorphs calcite, aragonite, and vaterite: An atomistic approach," J. Phys. Chem. B **102**, 2914–2922 (1998).

[27] A. G. Christy, "A review of the structures of vaterite: The impossible, the possible, and the likely," Cryst. Growth Des. **17**, 3567–3578 (2017).

[28] M. De La Pierre, P. Raiteri, and J. D. Gale, "Structure and dynamics of water at step edges on the calcite $\{10\bar{1}4\}$ surface," Cryst. Growth Des. **16**, 5907–5914 (2016).

[29] P. Raiteri, R. Demichelis, and J. D. Gale, "Thermodynamically consistent force field for molecular dynamics simulations of alkaline-earth carbonates and their aqueous speciation," J. Phys. Chem. C **119**, 24447–24458 (2015).

[30] Y. Wu, H. L. Tepper, and G. A. Voth, "Flexible simple point-charge water model with improved liquid-state properties," J. Chem. Phys. **124**, 024503–024513 (2006).

[31] E. Königsberger, L.-C. Königsberger, and H. Gamsjäger, "Low-temperature thermodynamic model for the system Na_2CO_3–$MgCO_3$–$CaCO_3$–H_2O," Geochim. Cosmochim. Acta **63**, 3105–3119 (1999).

[32] S. Fleming and A. Rohl, "GDIS: A visualization program for molecular and periodic systems," Z. Kristallogr. -Cryst. Mater. **220**, 580–584 (2005).

[33] X. Gan, K. He, B. Qian, Q. Deng, L. Lu, and Y. Wang, "The effect of glycine on the growth of calcium carbonate in alkaline silica gel," J. Cryst. Growth **458**, 60–65 (2017).

[34] J. D. Gale and A. L. Rohl, "The general utility lattice program (GULP)," Mol. Simul. **29**, 291–341 (2003).

[35] A. Klamt and G. Schüürmann, "COSMO: A new approach to dielectric screening in solvents with explicit expressions for the screening energy and its gradient," J. Chem. Soc., Perkin Trans. 2 **1993**, 799–805.

[36] J. D. Gale and A. L. Rohl, "An efficient technique for the prediction of solvent-dependent morphology: The COSMIC method," Mol. Simul. **33**, 1237–1246 (2007).

[37] S. Plimpton, "Fast parallel algorithms for short-range molecular dynamics," J. Comput. Phys. **117**, 1–19 (1995).

[38] P. Raiteri, general purpose trajectory analyser (GPTA), https://github.com/praiteri/GPTA, 2021.

[39] R. M. Brunne, E. Liepinsh, G. Otting, K. Wüthrich, and W. F. Van Gunsteren, "Hydration of proteins. A comparison of experimental residence times of water molecules solvating the bovine pancreatic trypsin inhibitor with theoretical model calculations," J. Mol. Biol. **231**, 1040–1048 (1993).

[40] R. W. Impey, P. A. Madden, and I. R. McDonald, "Hydration and mobility of ions in solution," J. Phys. Chem. **87**, 5071–5083 (1983).

[41] P. Geissbühler, P. Fenter, E. DiMasi, G. Srajer, L. B. Sorensen, and N. C. Sturchio, "Three-dimensional structure of the calcite–water interface by surface x-ray scattering," Surf. Sci. **573**, 191–203 (2004).

[42] P. Fenter, S. Kerisit, P. Raiteri, and J. D. Gale, "Is the calcite–water interface understood? Direct comparisons of molecular dynamics simulations with specular x-ray reflectivity data," J. Phys. Chem. C **117**, 5028–5042 (2013).

[43] S. J. T. Brugman, P. Raiteri, P. Accordini, F. Megens, J. D. Gale, and E. Vlieg, "Calcite (104) surface–electrolyte structure: A 3D comparison of surface X-ray diffraction and simulations," J. Phys. Chem. C **124**, 18564–18575 (2020).

[44] P. Raiteri, A. Schuitemaker, and J. D. Gale, "Ion pairing and multiple ion binding in calcium carbonate solutions based on a polarizable AMOEBA force field and ab initio molecular dynamics," J. Phys. Chem. B **124**, 3568–3582 (2020).